CrystEngComm

PAPER

View Article Online
View Journal | View Issue

# Synthesis and luminescence of uniform europium-doped bismuth fluoride and bismuth oxyfluoride particles with different morphologies†

Cite this: *CrystEngComm*, 2014, **16**, 3274

Alberto Escudero,*[a] Elisa Moretti[b] and Manuel Ocaña[a]

Facile synthesis routes have been developed for the preparation of uniform cubic bismuth fluoride and bismuth oxyfluoride particles. The synthesis methods are based on homogeneous precipitation reactions at 120 °C in solutions of bismuth nitrate and sodium tetrafluoroborate precursors in polyol-based solvents. Both the nature of the solvent and the heating modes (conventional or microwave-assisted heating) have a remarkable effect on the morphology and crystallinity of the resulting particles. Thus, polycrystalline spheres of α-$BiF_3$ with a mean diameter ranging from 1.2 to 2 μm could be obtained by heating solutions with the appropriate reagent concentrations in a mixture of ethylene glycol and glycerol (1 : 1 by volume) using a conventional oven, whereas octahedral single crystals of α-$BiO_yF_{3-2y}$ with mean edges ranging from 250 nm to 920 nm precipitated when using a diethylene glycol–water mixture (8 : 2 in volume) as solvent and a microwave reactor for heating. To explain these different morphological and structural features, the mechanism of formation of such particles was investigated. Both kinds of particles were also doped with $Eu^{3+}$, and both the morphological and luminescence properties of the resulting materials were evaluated. It was found that the luminescence intensity of the europium-doped α-$BiO_yF_{3-2y}$ nanoparticles was higher than that of the europium-doped α-$BiF_3$ sub-micrometric spheres, which was associated with the higher crystallinity of the former. Moreover, the presence of oxygen in the europium-doped α-$BiO_yF_{3-2y}$ samples permits the excitation of the europium cations through an Eu–O energy transfer process, which results in a much higher luminescence intensity with respect to that corresponding to the direct excitation of the europium cations. Finally, the effect of the amount of dopant on the luminescence properties of the phosphors was also evaluated.

Received 3rd December 2013,
Accepted 17th January 2014

DOI: 10.1039/c3ce42462f

www.rsc.org/crystengcomm

## 1. Introduction

The design of new methods for the synthesis of materials that yield uniform particles with controlled particle shape and size is of great importance in materials science from both the fundamental and technological points of view. This is a consequence of the strong effect that the morphology, size, and structure of the particles may have on many physicochemical properties of materials (electronic, magnetic, optical, *etc.*).[1–4]

Bismuth fluoride ($BiF_3$) exhibits two different polymorphic structures, α-$BiF_3$ with a cubic fluorite-based structure (space group $Fm\bar{3}m$, no. 225)[5] and β-$BiF_3$ with orthorhombic symmetry (space group *Pnma*, no. 62), which is isostructural with $YF_3$.[6] Solid solutions of bismuth oxyfluorides $BiO_yF_{3-2y}$ based on the cubic fluorite, orthorhombic, monoclinic, rhombohedral, and hexagonal structures have been reported in the literature.[7–9] These fluorides have been used as positive electrode material for lithium batteries[10] and as catalysts,[11] among other uses. Interestingly, owing to the similarity between the ionic radius of $Bi^{3+}$ and that of lanthanide ($Ln^{3+}$) ions,[12] these materials could also find important applications as host matrices for doping with $Ln^{3+}$ cations yielding Ln-based phosphors, as it has been suggested for other bismuth compounds such as $BiPO_4$.[13] Fluoride-based matrices would be advantageous when compared to oxidic hosts due to their low phonon energy (<350 $cm^{-1}$), which involves a lower probability of nonradiative relaxation, and therefore improved quantum efficiency of the luminescence should be expected.[14,15] It should be noted that most of the fluoride matrices so far studied are those based on rare earth (Y, Ln) cations.[16–18] The substitution of these cations by $Bi^{3+}$ would be also advantageous from the economic point of view since Bi is easily available, easily purifiable and cheaper than the

[a] *Instituto de Ciencia de Materiales de Sevilla (CSIC-Universidad de Sevilla), C/Américo Vespucio 49, E-41092 Seville, Spain. E-mail: aescudero@icmse.csic.es*
[b] *Department of Molecular Sciences and Nanosystems, Ca' Foscari University of Venice, Via Torino, 155/B Mestre Venice, Italy*

† Electronic supplementary information (ESI) available: SEM micrographs of other bismuth fluoride and bismuth oxyfluoride particles mentioned in the text. See DOI: 10.1039/c3ce42462f

rare earths.[13] In spite of such advantages, very few studies have been reported regarding the synthesis of uniform particles consisting of bismuth-based fluorides. In fact, to the best of our knowledge, only Zhao *et al.* have recently described a synthesis method based on an acid–base-coupled extractant route that gives rise to β-$BiF_3$ nanocrystals with plate- and rod-like morphologies,[19] and Sarkar *et al.* have reported the synthesis of $Ln^{3+}$-doped cubic $BiF_3$ nanoparticles confined in a polymer matrix.[20]

We describe herein for the first time a facile method for the synthesis of highly uniform micrometric $BiF_3$ spheres and sub-micrometric $BiO_yF_{3-2y}$ octahedral particles with a cubic structure, which is based on a homogeneous precipitation in glycol media at 120 °C. We demonstrate that in this method, the nature of the solvent, the concentration of the reactants, and the heating source are the main factors governing the resulting particle size and shape. We also address the doping with $Eu^{3+}$ of both types of particles, aiming to obtain phosphors with red luminescence under UV irradiation. Finally, the luminescence properties of both kinds of phosphors are studied and comparatively analysed in relation to their different compositional and structural characteristics.

## 2. Experimental

### 2.1 Reagents

Bismuth nitrate pentahydrate ($Bi(NO_3)_3{\cdot}5H_2O$, Sigma, >99.99%), sodium tetrafluoroborate ($NaBF_4$ Sigma, >98.0%), and europium(III) nitrate pentahydrate ($Eu(NO_3)_3{\cdot}5H_2O$, Sigma, 99.9%) were used as bismuth, fluoride, and europium sources, respectively. Ethylene glycol (EG, Sigma, 99.8%), glycerol (GLY, Sigma, >99%), diethylene glycol (DEG, Sigma, 99.0%), and double-distilled water were used as solvents. All chemicals were used as received.

### 2.2 Synthesis of the particles

Both bismuth fluoride and bismuth oxyfluoride particles were synthesised by homogeneous precipitation at 120 °C in solutions having variable concentrations of bismuth nitrate and sodium tetrafluoroborate in different polyol-based solvents and using different heating modes, as summarized in Table 1. The experimental procedure varied slightly depending on the solvent and the heating mode selected. Thus, for the samples synthesised in pure glycols, $Bi(NO_3)_3{\cdot}5H_2O$ and $NaBF_4$ were dissolved separately in 5 mL of the corresponding solvent. When using EG–GLY mixtures, $Bi(NO_3)_3{\cdot}5H_2O$ was dissolved in GLY and $NaBF_4$ in EG. In the case of the samples synthesised using DEG–water mixtures, $Bi(NO_3)_3{\cdot}5H_2O$ was dissolved in DEG, whereas $NaBF_4$ was dissolved in $H_2O$. All of the glycol solutions were magnetically stirred while mildly heating at low temperature (~75 °C) to favour dissolution. After cooling down to room temperature, the solutions containing the $Bi^{3+}$ and $F^-$ precursors were mixed, homogenized, and finally heated either in a conventional oven for 15 hours or in an Anton Paar Monowave 300 microwave synthesis reactor with a heating rate of 30 °C $min^{-1}$. In the latter case, the reaction was stopped just after reaching the target temperature. After finishing the heating process and cooling down to room temperature, the obtained suspensions were centrifuged to remove the supernatants, and the precipitates were washed twice with ethanol and once with double-distilled water. The so obtained particles were finally dispersed in double-distilled water or dried at room temperature in order to carry out further characterization. The study of the mechanism of particle formation was carried out by analysing the precipitates obtained after different aging times.

Europium-doped particles were prepared following the same methodology described for the undoped samples but adding the appropriate amount of $Eu(NO_3)_3{\cdot}5H_2O$ to the initial $Bi(NO_3)_3{\cdot}5H_2O$ solutions (Table 2).

**Table 1** Morphology and size of the particles obtained by aging at 120 °C in solutions containing $Bi(NO_3)_3$ and $NaBF_4$ under different experimental conditions. CH = conventional heating for 15 hours; MW = microwave-assisted treatment. The size corresponds to the main dimensions of the particles (diameter or edges). Numbers in parentheses indicate standard deviations

| Sample | $[Bi(NO_3)_3\ 5H_2O]$ (M) | $[NaBF_4]$ (M) | mL EG | mL glycerol | Treatment | Morphology | Size (μm) |
|---|---|---|---|---|---|---|---|
| BiF1 | 0.02 | 0.02 | 10 | 0 | CH | Quasispheres | 3.1(0.8) |
| BiF2 | 0.02 | 0.02 | 8 | 2 | CH | Quasispheres | 2.1(0.3) |
| BiF | 0.02 | 0.02 | 5 | 5 | CH | Spheres | 1.2(0.2) |
| BiF3 | 0.02 | 0.02 | 3 | 7 | CH | Heterogeneous | |
| BiF4 | 0.05 | 0.05 | 5 | 5 | CH | Polydisperse spheres | 2.0 (1.0) |
| BiF5 | 0.01 | 0.01 | 5 | 5 | CH | Polydisperse and agglomerated spheres | |
| BiF6 | 0.02 | 0.04 | 5 | 5 | CH | Spheres | 1.7 (0.1) |
| BiF7 | 0.02 | 0.08 | 5 | 5 | CH | Spheres | 2.0 (0.1) |
| BiF8 | 0.02 | 0.02 | 5 | 5 | MW | Agglomerated | |

| Sample | $[Bi(NO_3)_3\ 5H_2O]$ (M) | $[NaBF_4]$ (M) | mL DEG | mL H2O | Treatment | Morphology | Size (μm) |
|---|---|---|---|---|---|---|---|
| BiOF1 | 0.02 | 0.02 | 10 | 0 | MW | Heterogeneous | |
| BiOF2 | 0.02 | 0.02 | 8 | 2 | MW | Octahedra | 0.71 (0.28) |
| BiOF3 | 0.05 | 0.05 | 8 | 2 | MW | Octahedra | 0.92 (0.25) |
| BiOF | 0.02 | 0.15 | 8 | 2 | MW | Octahedra | 0.25 (0.01) |
| BiOF4 | 0.02 | 0.50 | 8 | 2 | MW | Agglomerated | |
| BiOF5 | 0.02 | 0.15 | 8 | 2 | CH | Heterogeneous | |

Table 2 Nominal and ICP-determined europium content (Eu/Eu + Bi mol ratio), morphology, size (diameter or edge), unit cell parameters and crystallite size of the europium-doped bismuth fluoride and bismuth oxyfluoride particles. Data corresponding to undoped particles are also shown for comparison. Numbers in parentheses indicate standard deviations (particle size) or absolute errors (unit cell parameter)

| Sample | Eu/Eu + Bi mol ratio (nominal) (%) | Eu/Eu + Bi mol ratio (ICP) (%) | Morphology | Size | Unit cell parameter (Å) | Crystallite size (nm) |
|---|---|---|---|---|---|---|
| BiF | | | Spheres | 1.20 (0.20) μm | 5.8344(9) | 49 |
| EuBiF | 2.5 | 2.52 | Spheres | 0.80 (0.10) μm | 5.827(1) | 38 |
| BiOF | | | Octahedra | 250 (10) nm | 5.8131(3) | >100 |
| EuBiOF1 | 2.5 | 2.67 | Octahedra | 81(5) nm | 5.8058(5) | 80 |
| EuBiOF2 | 5 | 5.17 | Octahedra | 87 (8) nm | 5.8021(7) | 81 |

### 2.3 Characterization

Particle shape was examined by scanning electron microscopy (SEM-FEG Hitachi S4800). Particle size distributions were obtained from the SEM micrographs by counting about one hundred particles. The qualitative chemical composition of the particles was studied by energy dispersive X-ray analysis (EDX) using a Philips DX4 attached to a transmission electron microscope (TEM, Philips 200 CM). Semiquantitative determination of the fluorine content was carried out by X-ray fluorescence (XRF) using a Panalytical (AXIOS) spectrometer. Bismuth and europium contents were assessed by induced coupled plasma atomic emission spectroscopy (ICP-AES) using an ICP Horiba Jobin Yvon Ultima 2 spectrometer, for which the particles were dissolved in concentrated HCl. Infrared spectra (FTIR) of the particles diluted in KBr pellets were recorded using a Jasco FT/IR-6200 Fourier transform spectrometer. X-ray diffraction (XRD) studies were carried out using a Panalytical, X'Pert Pro diffractometer equipped with an X-Celerator detector over an angular range of $10° < 2\theta < 120°$, a step width of 0.02°, and a 1000 s counting time. The patterns were analysed using the Le Bail algorithm of the program package X'Pert HighScore Plus to determine the unit cell parameters. The crystallite sizes for several crystallographic directions ((111), (200), (220), and (311) planes) were determined by using the Scherrer formula. A value of 0.9 for the $K$ shape factor was employed.

Excitation and emission spectra of aqueous dispersions of the europium-doped particles (3 mg $cm^{-3}$) were recorded using a Horiba Jobin-Yvon Fluorolog FL3-11 spectrofluorometer operating in the front face mode. No perceptible signals of sedimentation were observed in both suspensions at least during the measurement time. The photograph showing the samples' luminescence was taken under illumination with ultraviolet radiation ($\lambda$ = 254 nm), filtered from an Hg discharge lamp.

## 3. Results and discussion

### 3.1 Synthesis and morphology of the particles

It has been amply reported that to obtain uniform particles by precipitation, this process must take place homogeneously, which can be achieved through the slow and controlled release of the precipitating anions or cations within the solution, so that the reaction kinetics is constant during the whole process.[21] In this work, $NaBF_4$ has been selected as the fluoride source, since the $BF_4^-$ anions are known to decompose on heating liberating the fluoride anions required for the precipitation of fluoride phases.[22,23] Moreover, bismuth is known to form complexes with polyols, which are very stable at room temperature,[24,25] so that these complexes may act as the Bi reservoir from which Bi cations are further released on heating. Therefore, the homogeneous precipitation strategy here described involves the controlled release of both anions and cations.

It is also well known that to obtain uniform particles by homogeneous precipitation, a specific reaction kinetics is also required, which is established after an analysis of the effects of the experimental reaction parameters on the morphological features of the precipitated particles.[21] The results obtained for such an analysis in our case are summarized in Table 1. As observed, polygonal particles with a quasi-spherical morphology having a mean diameter of 3.1 μm and a rather broad size distribution (standard deviation 0.8 μm) (Fig. 1A) were obtained by aging at 120 °C for 15 h solutions of $Bi^{3+}$ (0.02 M) and $NaBF_4$ (0.02 M) in ethylene glycol in a conventional oven (sample BiF1). The addition of glycerol to ethylene glycol while keeping constant the other experimental parameters produced slight changes in both the morphology and size of the precipitated particles. Thus, as the GLY/EG ratio is increased up to a value of 1 : 1 by volume (sample BiF), the particles (Fig. 1B) became more spherical, smaller, and more uniform. Thus, the resulting precipitate consisted of spheres with a mean diameter of 1.3 μm and standard deviation of 0.1 μm, although a small amount of smaller spheres with diameters around 400 nm was also present, resulting in an average diameter of 1.2 μm (standard deviation of 0.2 μm). A further increase in the relative amount of glycerol gave rise to a heterogeneous sample (sample BiF3) consisting of polydisperse spheres and agglomerated irregular particles (Fig. S1A†). The precursor concentrations in the starting solutions were also found to play a key role in the final morphology of the particles, since an increase in both $Bi^{3+}$ and $NaBF_4$ concentrations up to 0.05 M, keeping constant the other experimental conditions (sample BiF4), gave rise to polydisperse spheres with sizes ranging from 200 nm to 2.5 μm (Fig. S1B†), while a decrease in such concentrations (sample BiF5) resulted in aggregates of smaller spheres of about 600 nm in diameter (Fig. S1C†). It is also noteworthy that the size of the spheres could be tuned by altering the $NaBF_4/Bi^{3+}$ ratio. Thus, the mean diameter progressively

 

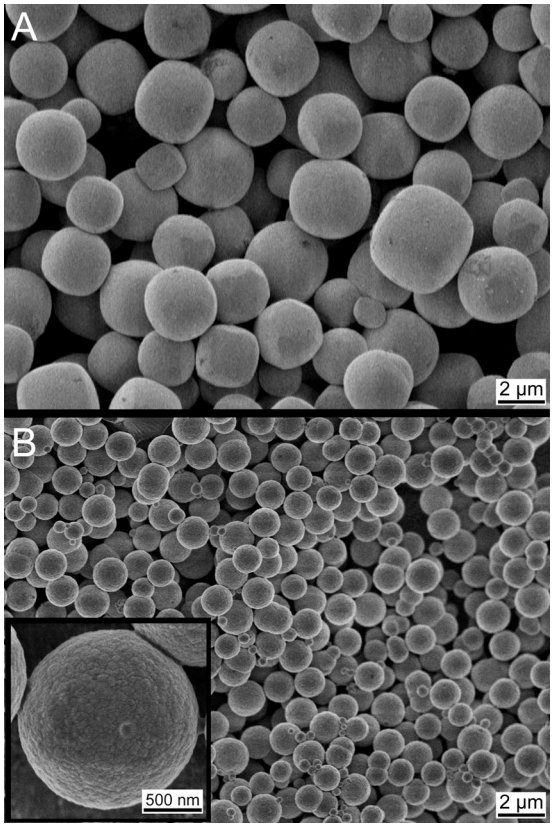


Fig. 1 SEM micrographs of the BiF1 (A) and BiF (B) samples.

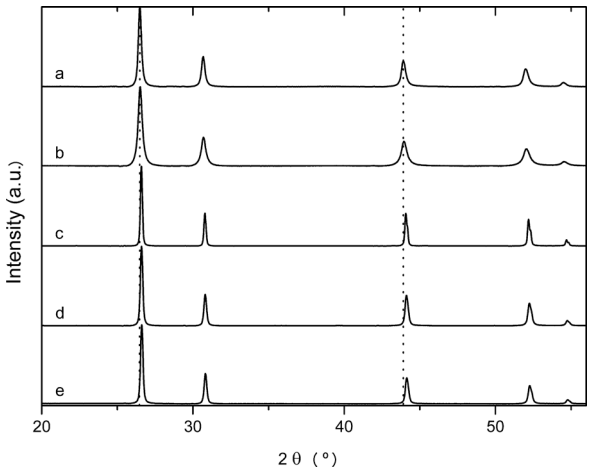


Fig. 2 XRD patterns of the BiF (a), EuBiF (b), BiOF (c), EuBiOF1 (d), and EuBiOF2 (e) samples. The vertical lines are guides for the eye.

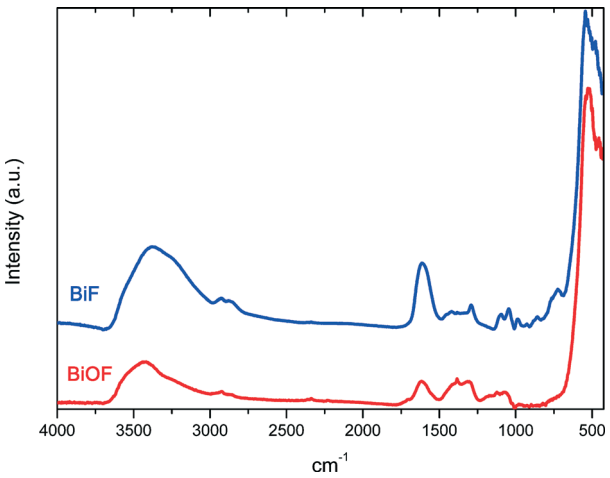


Fig. 3 FTIR spectra of the BiF and BiOF samples.

increased up to 2 μm as such a ratio was increased from 1 to 4 (sample BiF7).

Finally, it was found that when a microwave reactor was used for heating instead of a conventional oven (sample BiF8), very tiny, irregular, and agglomerated particles were obtained (Fig. S1D†), indicating that the heating source is in this case a crucial parameter to determine the final morphology of the particles. This behaviour might be related to the strong influence of this parameter on the precipitation rate, which is much faster in the microwave-assisted case.[26,27]

As illustrated for sample BiF, the spheres consisted of cubic α-$BiF_3$ (PDF 73-1988), as it can be inferred from the XRD pattern (Fig. 2a). The crystallite size estimated by using the Scherrer formula for this sample yielded a much lower value (49 nm) than the dimensions of the spheres. This finding strongly indicated that the spheres were polycrystalline, in agreement with their observation at high magnification under the SEM microscope (Fig. 1B, inset), which revealed a rough surface in which much smaller strongly aggregated particles seem to be identified.

The FTIR spectrum of this sample (Fig. 3) was also compatible with the $BiF_3$ composition, since it displayed the expected Bi–F stretching vibrations (around 530 $cm^{-1}$).[7] This spectrum also showed broad bands at 3400 and 1600 $cm^{-1}$ corresponding to adsorbed water and some other features which could be attributed to adsorbed glycols (around 1050 and 1100 $cm^{-1}$, ascribed to the C–O stretching modes, and around 1400, 2880, and 2930 $cm^{-1}$, due to the scissor and the symmetric and asymmetric stretching vibrations of $CH_2$ groups, respectively).[28,29] These observations seem to indicate the formation of stable bismuth–glycol complexes in the starting solutions, which act as a reservoir of the bismuth ions, as above indicated.

When heating $Bi^{3+}$ (0.02 M) and $BF_4^-$ (0.02 M) solutions using pure DEG as the solvent and a microwave reactor as the heating source (sample BiOF1), irregular particles were obtained (Fig. 4A). However, the addition of a small amount of water to the DEG solvent had an important effect on the morphology of the particles. Thus, for a DEG/water ratio of 8 : 2 (by volume) (sample BiOF2), octahedral particles, with a mean edge of 710 nm and slightly polydisperse (standard deviation of 280 nm), were obtained (Fig. 4B). An increase in the precursor concentration up to 0.05 M (keeping the $Bi^{3+}/NaBF_4$ ratio = 1) (sample BiOF3) produced slightly larger octahedra with a mean edge of 920 nm (standard deviation = 250 nm) (Fig. S2A†). Particle size could be also tuned in this

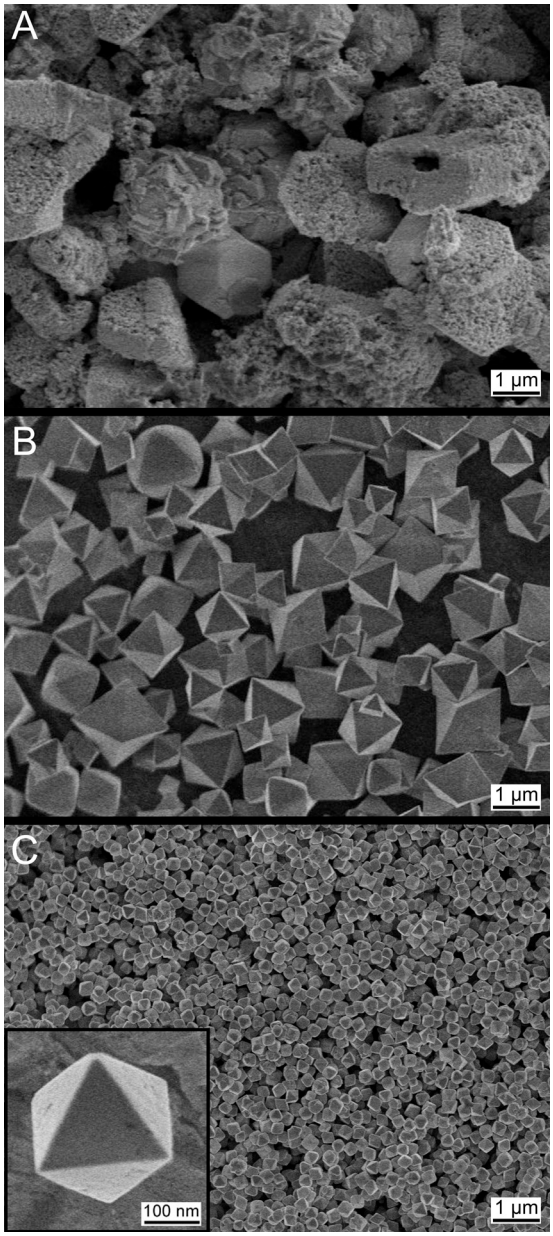


Fig. 4 SEM micrographs of the BiOF1 (A), BiOF2 (B), and BiOF (C) samples.

case by increasing the $NaBF_4/Bi^{3+}$ ratio, since octahedral particles with a mean edge of 250 nm and highly homogeneous (standard deviation = 10 nm) (Fig. 4C) were obtained by increasing such a ratio from 1 to 7.5 (sample BiOF). A further increase in such a ratio (sample BiOF4) gave rise to strongly agglomerated particles (Fig. S2B†). Finally, in this system, the heating source also played a key role on the final morphology of the particles, since heterogeneous and agglomerated particles (Fig. S2C†) resulted when heating in a conventional oven (sample BiOF5).

The XRD pattern of sample BiOF (Fig. 2c) also matched the PFD pattern 73-1988, corresponding to cubic α-$BiF_3$. However, the peaks appeared slightly shifted toward higher $2\theta$ angles, resulting in a unit cell parameter of 5.8131 Å, which was smaller than that obtained (5.8344 Å) for the $BiF_3$ spheres (sample BiF). It has been reported that the incorporation of some amount of oxygen into the original α-$BiF_3$ cubic structure gives rise to the formation of $BiO_yF_{3-2y}$ solid solutions. In fact, a cubic fluorite $CaF_2$ structure is known to occur for the $BiF_3$–$Bi_2O_3$ system for compositions ranging from pure $BiF_3$ to at least $BiO_{0.60}F_{1.80}$.[8] Within this compositional range, increasing the amount of oxygen produces very similar XRD patterns with signals shifting toward higher $2\theta$ angles, indicating shrinking of the unit cell. Therefore, the smaller value of the $a$ unit cell parameter of sample BiOF, compared with sample BiF, can be explained by the incorporation of oxygen into the $BiF_3$ lattice, resulting in a bismuth oxyfluoride. Such behaviour is consistent with the presence of water in the reaction medium, which promotes the hydrolysis of the $Bi^{3+}$ cations.[30,31] Further evidence for the incorporation of oxygen into the $BiF_3$ structure was assessed by means of chemical analysis by XRF, which gave a F/Bi ratio of sample BiOF of 2.30, to be compared with a value of 3.2 obtained for sample BiF. It should also be mentioned that the width of the XRD signals was much narrower than in sample BiF, which indicated a larger crystallite size. The average crystallite size obtained after applying the Scherrer formula (115 nm) was above the sensibility of the technique (<100 nm). However, taking into account the particle size observed by SEM, and the faceted octahedra of the particles, it can be reasonably assumed that the particles were likely single crystals.

As in the $BiF_3$ spheres, the FTIR spectrum of sample BiOF also displayed bands due to adsorbed DEG (Fig. 3), suggesting the formation of Bi–DEG complexes in the starting solutions.

### 3.2 Mechanisms of particle formation

Aiming to explain the differences observed in the shape and size of the particles when modifying the solvent nature and the reagent concentrations, their mechanisms of formation were investigated by monitoring the characteristics of the precipitates obtained after different aging times.

In the case of the synthesis of the $BiF_3$ spheres (sample BiF), a slight turbidity was detected after 30 min of aging, which was due to the formation of a gel-like precipitate (Fig. 5A). According to the XRD pattern (not shown), this precipitate consisted of aggregated $BiF_3$ tiny particles with a mean crystallite size of 48 nm. With an increase in the reaction time (90 minutes), solid aggregates with spherical shape, which seemed to be formed by the adhesion of the tiny particles, were observed (Fig. 5B). For longer aging times (5 hours), the size of the spherical particles increased, whereas the amount of tiny particles decreased (Fig. 5C). Finally, after 15 hours, only spheres were present (Fig. 1B). Longer aging times did not have a significant effect on the size and shape of the particles, indicating that they were completely formed after 15 hours of treatment. Taking into account that the crystallite size remained unaltered during the whole growth process, independent on the size of the spherical aggregates,

 

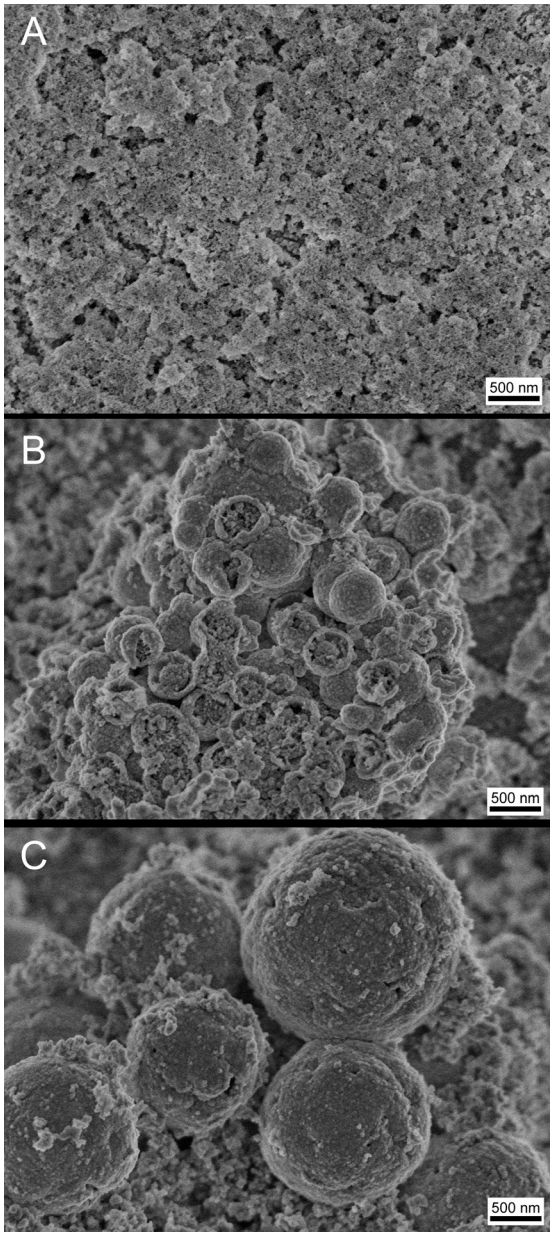


Fig. 5 SEM micrographs of the samples synthesised in EG : glycerol media (volume ratio 1 : 1) at 120 °C in a conventional oven for 30 minutes (A), 90 minutes (B), and 5 h (C).

the $BiF_3$ spheres seemed to grow by self-assembly of the initially formed particles. This growth mechanism by ordered aggregation of smaller subunits (primary particles) has been previously observed for many other systems obtained by homogeneous precipitation in different solvents, including polyols.[32–36] Such a mechanism of particle growth may explain, at least qualitatively, the different morphological characteristics (shape and especially size) of the $BiF_3$ particles precipitated under different experimental conditions, since the characteristics of the aggregation process in a colloidal system depend on the balance between attractive and repulsive forces, which are determined, among other factors, by the ionic strength (reagent concentrations) and the dielectric constant of the solvent[37] (37 and 42.5 for EG and GLY at 25 °C, respectively). The decrease in particle size observed as the amount of GLY in the solvent mixture was increased may also be ascribed to the consequent increase in viscosity (viscosity values of glycerol and EG at 20 °C are 1412 and 16.9, mPa s, respectively), which slows down the diffusion rate of the primary $BiF_3$ particles required for their self-assembly.

The octahedral particles of sample BiOF seemed to follow a different formation process. In fact, these particles were already formed just after reaching the target temperature, and no substantial changes in both their shape and the size were observed when increasing the aging time at 120 °C up to at least 30 minutes (not shown). This indicated that the synthesis process was extremely fast, which is one of the main advantages of the microwave-assisted protocols.[26,27] Despite this hinders any comprehensive study of the mechanism of the particle formation, they are very likely to be formed by a diffusion controlled growth mechanism, in which the particles are formed by the diffusion of solutes from the solution to the nuclei surface.[38] In these cases, the particle morphology is usually determined by the crystal habits corresponding to the crystal system,[39] cubic in our case, explaining the obtained octahedral shape. The decrease in the particle size observed when increasing the $NaBF_4/Bi^{3+}$ ratio can be explained on the basis of the classical model of nucleation and crystalline growth proposed by LaMer.[40,41] Thus, as increasing the fluoride concentration with a constant bismuth amount, a faster nucleation rate is expected, which gives rise to an increase in the number of nuclei, and therefore, smaller particles must be obtained.

### 3.3 Synthesis and characterization of the europium-doped particles

To dope the uniform bismuth fluoride (sample BiF) and bismuth oxyfluoride (sample BiOF) particles with $Eu^{3+}$ ions, similar experimental protocols to those described above for the synthesis of the undoped samples were followed, with a slight modification consisting of the addition of europium nitrate to the starting solutions (Table 2).

As observed, in the case of the $BiF_3$ spheres, the addition of 2.5% of $Eu^{3+}$ (Eu/Eu + Bi mol ratio) (sample EuBiF) resulted in uniform spherical particles similar to those obtained for the undoped system but showing a smaller size (average diameter of 800 nm, standard deviation of 100 nm), as illustrated in Fig. 6A. Attempts to further increase the europium content up to 5% failed, since polydisperse and aggregated spheres with sizes ranging from 350 nm to 1.5 μm were obtained (Fig. S3A†).

For the bismuth oxyfluoride octahedra, the presence of europium in the starting solutions up to 5% (sample EuBiOF2) had a slight effect not only on the final size of the particles, which decreased to 87 nm (standard deviation of 8 nm), but also on the shape of the particles, which exhibited slightly rounded borders and edges and were slightly aggregated (Fig. 6B). Higher levels of doping gave rise to

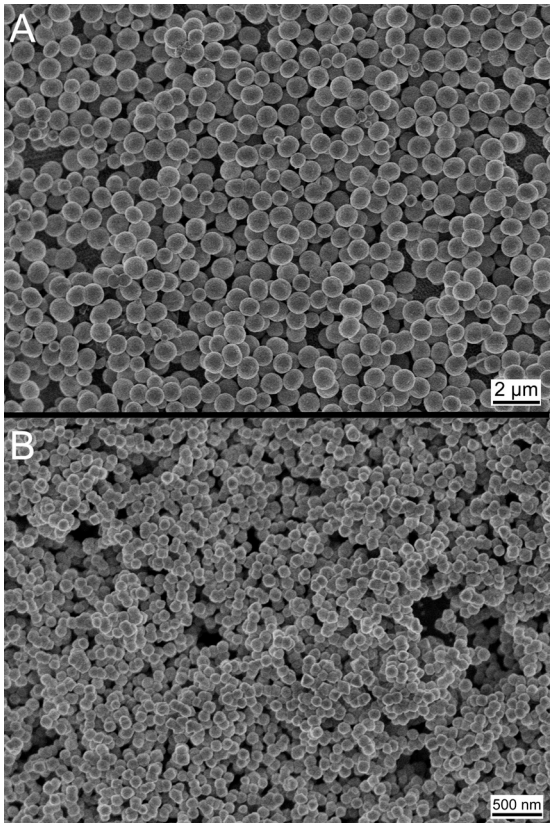


Fig. 6 SEM micrographs of the europium-doped EuBiF (A) and EuBiOF2 samples.

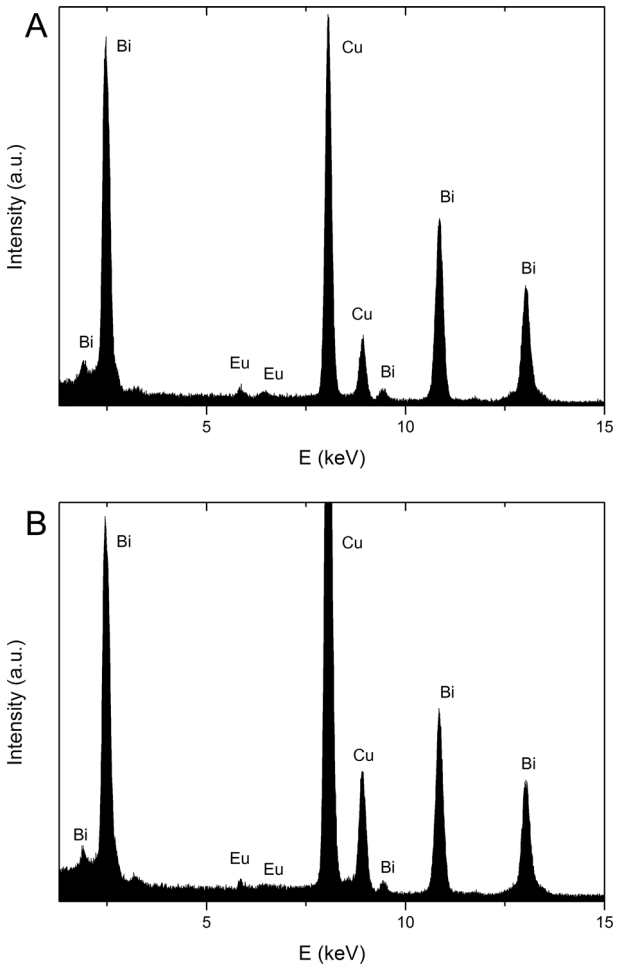


Fig. 7 EDX spectra of single particles corresponding to the EuBiF (A) and EuBiOF1 (B) samples.

polydisperse and agglomerated quasispheres (Fig. S3B†). It should be noted that a similar decrease in the particle size on doping with lanthanide ions has been previously reported for the case of some rare earth fluorides. This was ascribed to surface charge modifications as a result of doping, which substantially affects the diffusion of negatively-charged fluoride ions into the particle surface and therefore, the crystal growth rate.[42,43]

Evidence of the incorporation of europium into the spherical and octahedral particles was obtained from EDX spectra recorded for single particles in each case, which displayed low intensity europium peaks, in addition to those of bismuth (Fig. 7). ICP-AEP measurements indicated that the experimental Eu/(Eu + Bi) molar ratios corresponding to the doped particles were in good agreement with the nominal values (Table 2), thus indicating the quantitative incorporation of europium into the bismuth fluoride and oxyfluoride matrices. Further confirmation of the incorporation of $Eu^{3+}$ into the bismuth fluoride and bismuth oxyfluoride lattices was afforded by XRD. The diffraction patterns of the europium-doped samples (EuBiF, EuBiOF1, and EuBiOF2, Fig. 2b, d, and e) were very similar to those corresponding to the undoped counterparts (Fig. 2a and c), but with the peaks slightly shifted toward higher $2\theta$ angles, indicating a contraction of the unit cell. This was confirmed by the decrease in the unit cell parameter of the doped samples, compared to the undoped particles (Table 2). In addition, in the case of the bismuth oxyfluoride octahedra, a progressive decrease in the cubic unit cell parameter with an increase in the europium doping level was observed. This behaviour is in agreement with an isomorphic substitution of $Bi^{3+}$ cations by $Eu^{3+}$, which shows a slightly smaller ionic radius in eightfold coordination (1.07 Å) when compared to that of $Bi^{3+}$ (1.17 Å).[12]

The analysis of the peak width by using the Scherrer formula gave rise to an average crystallite size of 38 nm for sample EuBiF, much smaller than the particle size, indicating thus that the europium-doped spheres were also polycrystalline. Average crystallite values of 80 and 81 nm were calculated for the EuBiOF1 and EuBiOF2 samples, respectively, giving clear evidence that the europium-doped octahedra were single crystals.

### 3.4 Optical properties of the europium-doped bismuth fluoride and bismuth oxyfluoride phosphors

In order to determine the effect of the composition and the morphology of the particles on their luminescence properties, excitation and emission spectra of aqueous suspensions

 

of the europium-doped samples were recorded. Excitation spectra of the EuBiF spheres and the EuBiOF1 octahedra, containing the same amount of europium (2.5% mol), were recorded by monitoring at a wavelength of 591 nm, which corresponds to the emission line expected for the $^5D_0 \rightarrow {}^7F_1$ transition of $Eu^{3+}$.[44] Both spectra (Fig. 8A) exhibited several sharp bands above 310 nm, which correspond to the direct excitation of the $Eu^{3+}$ ions from the ground state $^7F_0$ to the different excited levels. The most intense one appearing at 393 nm is associated with the $^7F_0 \rightarrow {}^5L_6$ transition, as it has been widely reported in the literature for other $Eu^{3+}$ based phosphors.[26,35,45] The excitation spectrum of sample EuBiOF1 showed an intense extra broad excitation band centred at 275 nm, which did not appear on the spectrum of the EuBiF spheres. This band could be assigned to an Eu–O charge-transfer band (CTB), arising from the transition of the 2p electrons of $O^{2-}$ to the empty 4f orbitals of $Eu^{3+}$ ions, following the previous studies on the lanthanide-doped lanthanide oxyfluorides.[46,47] The negligible intensity of this band in the excitation spectrum of the EuBiF particles was in agreement with the absence of a significant amount of oxygen impurities in the $BiF_3$ samples.

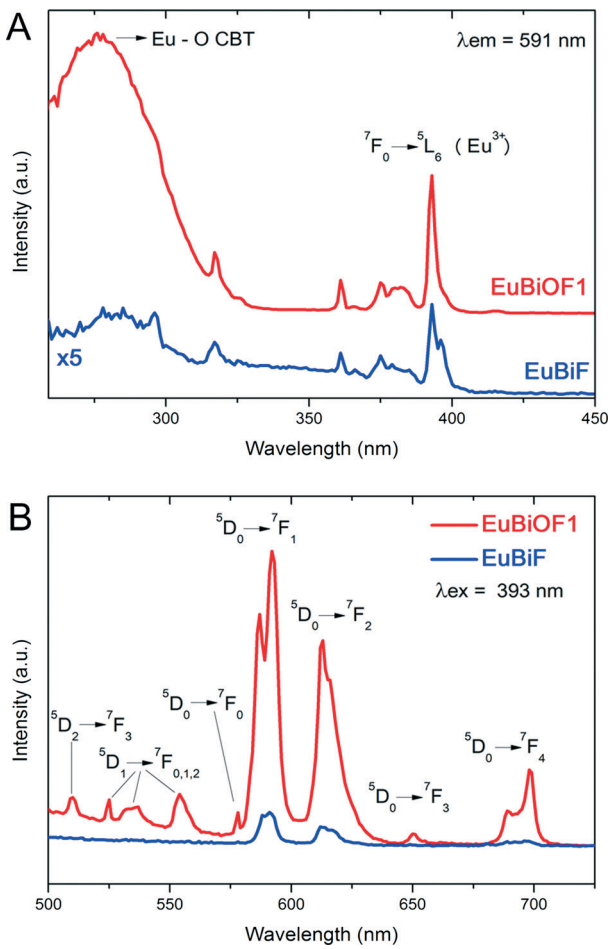


**Fig. 8** (A) Excitation spectra ($\lambda_{em}$ = 591 nm) of aqueous suspensions of the EuBiOF1 and EuBiF samples. Note that the intensities of the EuBiF sample have been multiplied by 5 in order to better visualize the signals. (B) Emission spectra ($\lambda_{ex}$ = 393 nm) of aqueous suspensions of the EuBiOF1 and EuBiF samples.

The emission spectra obtained for samples EuBiF and EuBiOF1 under the direct UV excitation of europium (393 nm) displayed the typical emissions in the 570–700 nm region, which correspond to the $^5D_0 \rightarrow {}^7F_J$ ($J$ = 0, 1, 2, 3, and 4) electronic transitions expected for the $Eu^{3+}$ cation[44] (Fig. 8B). It can also be observed that the relative emission intensity of the band centred at 591 nm ($^5D_0 \rightarrow {}^7F_1$ transition) showed for both samples is higher than that associated with the $^5D_0 \rightarrow {}^7F_2$ transition appearing at 612 nm. This is normally associated with $Eu^{3+}$ cations occupying crystallographic sites with an inversion center,[48] which is compatible with the replacement of $Bi^{3+}$ by $Eu^{3+}$ cations, since in the cubic α-$BiF_3$ and α-$BiO_yF_{3-2y}$ structures the bismuth site shows a $O_h$ local symmetry.[5] Surprisingly, a weak band corresponding to the $^5D_0 \rightarrow {}^7F_0$ transition (578 nm), which is not allowed for $Eu^{3+}$ in centrosymmetric sites, is also observed on the spectra. However, this band has been previously observed for $Eu^{3+}$ in other matrices with similar local symmetry and attributed to the presence of some $Eu^{3+}$ ions at defect sites in the crystal.[49] Bands appearing from 500 to 560 nm associated with transitions from the $^5D_1$ and $^5D_2$ upper excited states of $Eu^{3+}$ to the $^7F_J$ levels[50] could also be observed in the spectrum of sample EuBiOF1. These bands usually appear in matrices with a very low phonon energy in which the probability of quenching by multiphonon relaxation is low,[51] thus indicating that bismuth oxyfluoride is a very convenient matrix to be doped with luminescent lanthanide cations. It is also outstanding that the intensity of the bands corresponding to the EuBiOF1 phosphors was above one order of magnitude higher than that exhibited by the EuBiF particles. This behaviour can be associated with the higher crystallinity of the bismuth oxyfluoride octahedra, since crystalline defects are known to quench the luminescence of the lanthanide ions.[52,53]

It was also found that for the europium-doped bismuth oxyfluoride sample, the emission intensity increased around three times when exciting through the Eu–O CTB (275 nm), compared to the direct excitation of $Eu^{3+}$ at 393 nm (Fig. 9A), indicating that the former excitation path is more favourable for the potential applications of these phosphors.

Finally, the effect of the europium content on the luminescence of the most efficient phosphors (europium-doped bismuth oxyfluoride octahedra) was studied for an excitation wavelength of 275 nm (Fig. 9B). The increase in europium concentration from 2.5% to 5% mol gave rise to a notable increase in the emission intensity. In fact, the intensity of the emission bands corresponding to sample EuBiOF2 was about two times higher than that of the EuBiOF1 particles. Taking into account that the first sample contained two times europium emitting centers, no concentration quenching effects seemed to take place, at least up to a europium doping level of 5% mol. Therefore, the phosphors showing the best luminescence properties are those consisting of europium-doped bismuth oxyfluoride octahedral particles doped with 5% mol of europium, when excited though the Eu–O CTB at 275 nm.

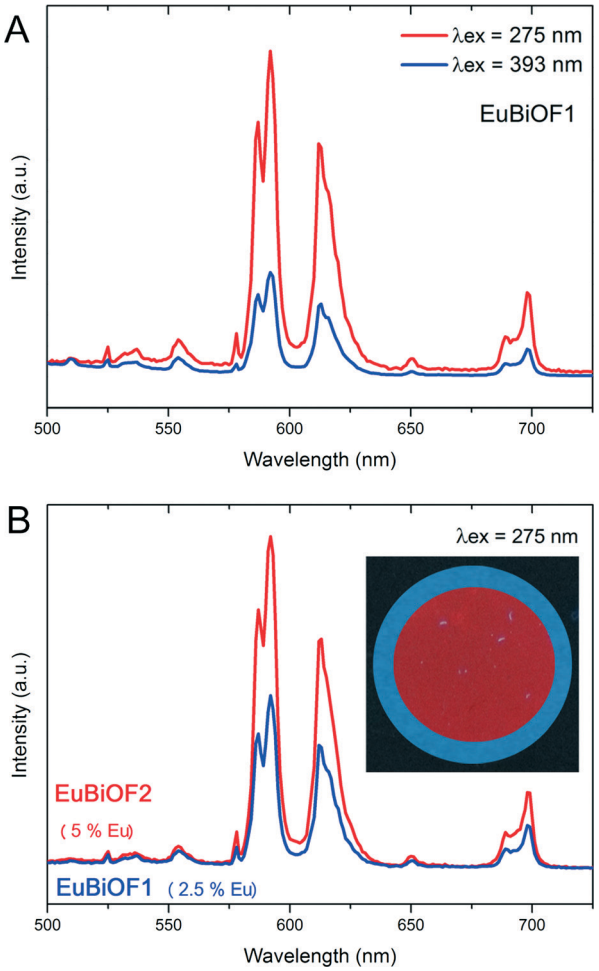


**Fig. 9** (A) Emission spectra of aqueous suspension of the EuBiOF1 sample for excitation wavelengths of 275 nm and 393 nm. (B) Emission spectra ($\lambda_{ex}$ = 275 nm) of aqueous suspensions of the EuBiOF2 and EuBiOF1 samples. The photograph of the inset shows the orange–red luminescence of sample EuBiOF2 when irradiated at 254 nm.

## 4. Conclusions

Bismuth fluoride ($BiF_3$) micrometric spheres of narrow size distribution have been synthesised by homogeneous precipitation reactions at 120 °C from bismuth nitrate and sodium tetrafluoroborate solutions using a mixture of ethylene glycol and glycerol (50% by volume) as a solvent and a conventional oven for heating, under a restrictive set of reagent concentrations. The mean diameters of the spheres could be tuned in from 1.2 to 2 μm by changing the $NaBF_4/Bi^{3+}$ ratio. These particles were polycrystalline and were formed though an aggregation process of smaller subunits. The change of the solvent nature, diethylene glycol–water mixtures (8 : 2 by volume), and the use of a microwave heating reactor instead of a conventional oven gave rise to bismuth oxyfluoride ($BiO_yF_{3-2y}$) octahedral single crystals formed by a diffusion-controlled growth mechanism. The size of these octahedra could be also varied from 250 to 920 nm (mean edge) depending on the $NaBF_4/Bi^{3+}$ ratio. Both kinds of particles were able to accommodate $Eu^{3+}$ into their structures without altering the uniformity of the particles, although their size decreased and their shape slightly changed in the case of the octahedra, as a consequence of doping. Both kinds of doped particles emitted red luminescence under UV illumination whose intensity was higher for the europium-doped bismuth oxyfluoride octahedra than for the europium-doped bismuth fluoride spheres, which was associated with the higher crystallinity of the former. Moreover, the presence of oxygen in the bismuth oxyfluoride particles gave rise to a charge transfer (at 275 nm) which could be used to excite the $Eu^{3+}$ cations more efficiently than through the direct excitation of the europium cations. Finally, the effect of the europium content on the luminescence properties of the latter system has been also studied, finding that the luminescence intensity increased as the Eu content was increased up to a Eu/Eu + Bi mol ratio of 5%, with no signs of concentration quenching effects.

## Acknowledgements

This work has been supported by the Junta de Andalucía (grant FQM 6090) and by the Spanish Ministerio de Ciencia e Innovación (MAT2011-23593). A.E. thanks the Spanish National Research Council (CSIC) and the Fondo Social Europeo (FSU) for a JAE-DOC contract. M. Carmen Jiménez and Paco Quesada (paco@pacoquesada.com) are gratefully acknowledged for the help with SEM and graphic design, respectively.

## Notes and references

1 S. Piana, M. Reyhani and J. D. Gale, *Nature*, 2005, **438**, 70–73.
2 J. Park, J. Joo, S. G. Kwon, Y. Jang and T. Hyeon, *Angew. Chem., Int. Ed.*, 2007, **46**, 4630–4660.
3 Y. N. Xia, P. D. Yang, Y. G. Sun, Y. Y. Wu, B. Mayers, B. Gates, Y. D. Yin, F. Kim and Y. Q. Yan, *Adv. Mater.*, 2003, **15**, 353–389.
4 A. P. Alivisatos, *Science*, 1996, **271**, 933–937.
5 F. Hund and R. Fricke, *Z. Anorg. Chem.*, 1949, **258**, 198–204.
6 A. F. Wells, *Structural Inorganic Chemistry*, 5th edn, Oxford Science Publications, 1984.
7 M. Bervas, B. Yakshinskiy, L. C. Klein and G. G. Amatucci, *J. Am. Ceram. Soc.*, 2006, **89**, 645–651.
8 F. V. Kalinchenko, M. P. Borzenkova and A. V. Novoselova, *Zh. Neorg. Khim.*, 1981, **26**, 222–225.
9 A. Morell, B. Tanguy and J. Portier, *Bull. Soc. Chim. Fr.*, 1971, 2502–2504.
10 M. Bervas, F. Badway, L. C. Klein and G. G. Amatucci, *Electrochem. Solid-State Lett.*, 2005, **8**, A179–A183.
11 *USA Pat.*, US 2795571 A, 1957.
12 R. Shannon, *Acta Crystallogr., Sect. A: Cryst. Phys., Diffr., Theor. Gen. Crystallogr.*, 1976, **32**, 751–767.
13 B. S. Naidu, B. Vishwanadh, V. Sudarsan and R. K. Vatsa, *Dalton Trans.*, 2012, **41**, 3194–3203.
14 W. Zheng, S. Zhou, Z. Chen, P. Hu, Y. Liu, D. Tu, H. Zhu, R. Li, M. Huang and X. Chen, *Angew. Chem., Int. Ed.*, 2013, **52**, 6671–6676.

 

15 Z.-L. Wang, H. L. W. Chan, H.-L. Li and J. H. Hao, *Appl. Phys. Lett.*, 2008, **93**, 141106.
16 N. O. Núñez and M. Ocaña, *Nanotechnology*, 2007, 18.
17 S. Rodríguez-Liviano, N. O. Núñez, S. Rivera-Fernández, J. M. de la Fuente and M. Ocaña, *Langmuir*, 2013, **29**, 3411–3418.
18 M. Nyk, R. Kumar, T. Y. Ohulchanskyy, E. J. Bergey and P. N. Prasad, *Nano Lett.*, 2008, **8**, 3834–3838.
19 J. M. Zhao, H. L. Pan, X. He, Y. S. Wang, L. Gu, Y. S. Hu, L. Q. Chen, H. Z. Liu and S. Dai, *Nanoscale*, 2013, **5**, 518–522.
20 S. Sarkar, A. Dash and V. Mahalingam, *Chem.–Asian J.*, 2014, **9**, 447–451.
21 E. Matijevic, *Chem. Mater.*, 1993, **5**, 412–426.
22 C. Li, J. Yang, P. Yang, H. Lian and J. Lin, *Chem. Mater.*, 2008, **20**, 4317–4326.
23 S. Sarkar and V. Mahalingam, *CrystEngComm*, 2013, **15**, 5750–5755.
24 Z. Liu, J. Liang, S. Li, S. Peng and Y. Qian, *Chem.–Eur. J.*, 2004, **10**, 634–640.
25 C. Fu, G. Li, M. Zhao, L. Yang, J. Zheng and L. Li, *Inorg. Chem.*, 2012, **51**, 5869–5880.
26 A. Escudero, M. E. Calvo, S. Rivera-Fernández, J. M. de la Fuente and M. Ocaña, *Langmuir*, 2013, **29**, 1985–1994.
27 S. Rodríguez-Liviano, F. J. Aparicio, T. C. Rojas, A. B. Hungría, L. E. Chinchilla and M. Ocaña, *Cryst. Growth Des.*, 2012, **12**, 635–645.
28 R. Chelli, F. L. Gervasio, C. Gellini, P. Procacci, G. Cardini and V. Schettino, *J. Phys. Chem. A*, 2000, **104**, 5351–5357.
29 W. Sawodny, K. Niedenzu and J. W. Dawson, *Spectrochim. Acta, Part A*, 1967, **23**, 799–806.
30 G. Gattow and D. Schott, *Z. Anorg. Allg. Chem.*, 1963, **324**, 31–47.
31 T. F. Bidleman, *Anal. Chim. Acta*, 1971, **56**, 221–231.
32 M. Ocaña, R. Rodriguez-Clemente and C. J. Serna, *Adv. Mater.*, 1995, **7**, 212–216.
33 S. Libert, V. Gorshkov, V. Privman, D. Goia and E. Matijević, *Adv. Colloid Interface Sci.*, 2003, **100–102**, 169–183.
34 Z. Zhang, H. Sun, X. Shao, D. Li, H. Yu and M. Han, *Adv. Mater.*, 2005, **17**, 42–47.
35 N. Núñez, J. Sabek, J. García-Sevillano, E. Cantelar, A. Escudero and M. Ocaña, *Eur. J. Inorg. Chem.*, 2013, **2013**, 1301–1309.
36 N. O. Núñez, S. Rodríguez-Liviano and M. Ocaña, *J. Colloid Interface Sci.*, 2010, **349**, 484–491.
37 V. Privman, D. V. Goia, J. Park and E. Matijević, *J. Colloid Interface Sci.*, 1999, **213**, 36–45.
38 J. A. Dirksen and T. A. Ring, *Chem. Eng. Sci.*, 1991, **46**, 2389–2427.
39 T.-D. Nguyen, *Nanoscale*, 2013, **5**, 9455–9482.
40 V. K. LaMer and R. H. Dinegar, *J. Am. Chem. Soc.*, 1950, **72**, 4847–4854.
41 V. K. LaMer, *Ind. Eng. Chem.*, 1952, **44**, 1270–1277.
42 F. Wang, Y. Han, C. S. Lim, Y. Lu, J. Wang, J. Xu, H. Chen, C. Zhang, M. Hong and X. Liu, *Nature*, 2010, **463**, 1061–1065.
43 D. Chen and Y. Wang, *Nanoscale*, 2013, **5**, 4621–4637.
44 F. S. Richardson, *Chem. Rev.*, 1982, **82**, 541–552.
45 M. Zhao, L. Li, J. Zheng, L. Yang and G. Li, *Inorg. Chem.*, 2012, **52**, 807–815.
46 M. Shang, D. Geng, X. Kang, D. Yang, Y. Zhang and J. Lin, *Inorg. Chem.*, 2012, **51**, 11106–11116.
47 T. Grzyb, M. Węcławiak, J. Rozowska and S. Lis, *J. Alloys Compd.*, 2013, **576**, 345–349.
48 J.-L. Adam, *Advanced Inorganic Fluorides: Synthesis, Characterization and Applications*, Elsevier, Switzerland, 2000.
49 P. A. Tanner, *Chem. Soc. Rev.*, 2013, **42**, 5090–5101.
50 P. Porcher and P. Caro, *J. Chem. Phys.*, 1976, **65**, 89–94.
51 J. Hölsä and E. Kestilä, *J. Chem. Soc., Faraday Trans.*, 1995, **91**, 1503–1509.
52 C. Ronda, *Luminescence: From Theory to Applications*, Wiley, Weinheim, 2008.
53 H. A. Höppe, *Angew. Chem., Int. Ed.*, 2009, **48**, 3572–3582.